INTERNATIONAL JOURNAL OF REMOTE SENSING, 2018
VOL. 39, NO. 8, 2105–2118
https://doi.org/10.1080/01431161.2017.1420929

Taylor & Francis
Taylor & Francis Group

A comparison of NDVI and EVI in the DisTrad model for thermal sub-pixel mapping in densely vegetated areas: a case study in Southern China

Jizhong Qiu[a,b,c], Jingxue Yang[d], Yunpeng Wang[a] and Hua Su[e]

[a]Guangzhou Institute of Geochemistry, Chinese Academy of Sciences, Guangzhou, China; [b]Bureau of Land and Resources of Chongzuo City, Chongzuo, China; [c]University of Chinese Academy of Sciences, Beijing, China; [d]Guangdong Research Institute of Water Resources and Hydropower, Guangzhou, China; [e]Key Laboratory of Spatial Data Mining and Information Sharing of Ministry of Education, National Engineering Research Centre of Geospatial Information Technology, Fuzhou University, Fuzhou, China

ABSTRACT

The DisTrad (Disaggregation Procedure for Radiometric Surface Temperature) model shows limited applicability for sub-pixel mapping of thermal remote-sensing images in densely vegetated areas due to the phenomenon of normalized difference vegetation index (NDVI) saturation. In this article, we compared the effect of NDVI and enhanced vegetation index (EVI) in the DisTrad model for thermal sub-pixel mapping in densely vegetated areas due to their different sensitivity in densely vegetated areas. Taking Ganzhou in Southern China as an example, we produced 250-m thermal remote-sensing images from a 1000-m image using 250-m NDVI and EVI data. After comparing with the synchronous 90-m thermal image from advanced spaceborne thermal emission and reflection radiometer, we found that the EVI can achieve a better result than NDVI in densely vegetated areas.

ARTICLE HISTORY
Received 15 September 2016
Accepted 12 December 2017

1. Introduction

Land surface temperature (LST) is a key variable in climate and environmental research. As an important impact factor of resources and environment, LST is essential for studying global agriculture, natural disasters, hydrology, ecology and the environment. In addition, LST offers broad application value in various domains, such as energy and water exchange among global crop assessment (Kogan 2001), coal fires (Deng, Wan, and Zhao 2001), earthquake forecasting (Lv, Ding, and Cui 2000), monitoring soil moisture status (Sandholt, Rasmussen, and Andersen 2002; Sun et al. 2012), land use and cover change (Lambin and Ehrlich 1996; Zhang and Wang 2006), as well as forest fires (Peng et al. 2007). Zakšek and Oštir (2012) analysed the diurnal cycle of urban heat island from LST images acquired from spinning enhanced visible and infrared imager. The traditional method to acquire LST is to measure temperature directly using instruments based on a land surface or platform, such as a meteorological station. This method can obtain continuous monitoring data with high precision covering small areas near the

CONTACT Yunpeng Wang wangyp@gig.ac.cn Guangzhou Institute of Geochemistry, Chinese Academy of Sciences, Guangzhou, China

station, but it is difficult to be used for temperature mapping in large-scale areas. The appearance of remote-sensing techniques shows possibilities to measure and map LST in large scales. However, until now, major obstacles still exist regarding mapping LST with both high-frequency and high-spatial resolution (e.g. 10–100 m) using satellite remote-sensing. Some remote-sensors have higher temporal resolutions but lower spatial ones, while some have higher spatial resolutions but lower temporal ones. Table 1 lists some thermal remote-sensors and their spatial and temporal resolutions. For example, moderate resolution imaging spectroradiometer (MODIS) can provide four thermal infrared images (two in the day and two in the night), but its spatial resolution is about 1000 m. Thermal image data of enhanced thematic mapper plus reach as high as 60 m, but its temporal resolution is only 16 days, which is insufficient for some applications. In general, images with 250–500 m resolution can meet the requirements of monitoring artificial land-use changes, and images with less than 500-m resolution are acceptable for monitoring globe change. Currently, enhancing spatial resolution remains the most efficient way to improve the applicability of thermal images. A simple way of improving the spatial resolution of thermal images is achieved through the UniTrad (uniform procedure for radiometric surface temperature) method (Kustas et al. 2003), which is a re-sampling method using algorithms, such as nearest neighbour interpolation, linear interpolation and cubic convolution interpolation. However, the accuracy of this method is not good due to its coarse algorithm. Kustas et al. (2003) proposed the DisTrad (disaggregation procedure for radiometric surface temperature) model to improve the spatial resolution of thermal images using the relationship between thermal infrared image data in a km scale and normalized difference vegetation index (NDVI) images in a hm scale, which makes it possible to fuse high-frequency LST data in a km scale and high-resolution LST data in a hm scale. The DisTrad model is commonly used in thermal sub-pixel mapping. The model first fitted a linear statistical relationship between LST and NDVI and then applied the relationship to NDVI image with high-spatial resolution. The final LST image with similar spatial resolution was obtained. However, NDVI is not always suitable for some regions with different coverage of vegetation. Agam et al. (2007) proposed the TsHARP (technique for spatial sharpening thermal image) algorithm by substituting NDVI in the original DisTrad model with F_c, which fit the relationship with LST. Using irrigated cropping area as study area, Merlin et al. (2010) modified the TsHARP algorithm by a green (photo-synthetically active) vegetation index (VI) that could disaggregate kilometric MODIS product at 100-m resolution successfully. Essa et al. (2012) evaluated the performance of a variety of indices in the DisTrad model, and they found that even if in urban areas covered by dense vegetation, index I (percentage impervious) was still much more effective than NDVI in the model. Zhan et al. (2013) divided the methods of disaggregation of remotely sensed LST into two categories: thermal sharpening and temperature unmixing. However, there is less research about the disaggregating LST in densely vegetated areas. The densely vegetated areas are widely distributed on the earth, but the NDVI saturation at high

Table 1. Spatial and temporal resolutions of sensors in some remote-sensing satellites.

Sensor	Satellite	Spatial resolution	Temporal resolution
TM	Landsat 5	30 m (120-m thermal)	16 days
ETM+	Landsat 7	30 m (60-m thermal, 15-m panchromatic)	16 days
MODIS	Terra and Aqua	250 m (2 bands), 500 m (5 bands), 1000 m (29 bands)	2 per day
AVHRR	NOAA	1.1 km	4 per day
GOES Imager	GOES	0.5–1 km (2–4 km thermal)	30 min
ASTER	Terra	90 m	16 days

biomass area limited its applicability for sub-pixel mapping of thermal remote-sensing images in densely vegetated areas.

In this article, taking Ganzhou in Southern China as a case, we compared the effect of NDVI and enhanced vegetation index (EVI) in the DisTrad model for thermal sub-pixel mapping in densely vegetated areas due to their different sensitivity in densely vegetated areas, and validated the results with 90-m resolution synchronous advanced spaceborne thermal emission and reflection radiometer (ASTER) data. The study discussed the applicability of NDVI and EVI in the DisTrad model in densely vegetated area, aiming to provide reference to thermal sub-pixel mapping.

2. Method and data

2.1. *DisTrad-NDVI and DisTrad-EVI method*

The DisTrad model proposed by Kustas et al. (2003) improves the spatial resolution of LST through a relationship between coarse NDVI and surface temperature (T_R) (R stands for 'radiometric') by the least-squares fitting method, which is named the DisTrad-NDVI method in this study. For solving the problem of over-saturation in densely vegetated areas, Agam et al. (2007) proposed a method replacing NDVI with the index of fractional vegetation cover (F_c) in the DisTrad model, which is named the DisTrad-F_c model in this study.

NDVI is a ratio based on the spectral reflectance from vegetation. NDVI is from combined operations between the red band and near infrared band, which is expressed mathematically as:

$$\mathrm{NDVI} = (R_{\mathrm{NIR}} - R_{\mathrm{Vis}})/(R_{\mathrm{NIR}} + R_{\mathrm{Vis}}) \tag{1}$$

where R_{NIR} stands for the spectral reflectance in the near infrared band (700–1100 nm); and R_{Vis} stands for the spectral reflectance of the visible band (400–700 nm). Calculations of NDVI for a given pixel always result in a number that ranges from minus one (−1) to plus one (+1); however, no green leaves give a value close to zero. A zero means no vegetation, and close to +1 (0.8–0.9) indicates the highest possible density of green leaves (NASA 2013). Fractional vegetation cover (F_c) is another integrated quantitative index for vegetation conditions, which is mathematically expressed as (Choudhury et al. 1994):

$$F_c = 1 - (\mathrm{NDVI}_{\max} - \mathrm{NDVI}/\mathrm{NDVI}_{\max} - \mathrm{NDVI}_{\min})^{0.625} \tag{2}$$

EVI is an 'optimized' index designed to enhance the vegetation signal with improved sensitivity in high biomass regions and improve vegetation monitoring through a decoupling of the canopy background signal and a reduction in atmosphere influences. EVI is computed as follows (Huete et al. 2002):

$$\mathrm{EVI} = G \times ((R_{\mathrm{NIR}} - R_{\mathrm{red}})/(R_{\mathrm{NIR}} + C_1 \times R_{\mathrm{red}} - C_2 \times R_{\mathrm{blue}} + L)) \tag{3}$$

where R_{NIR}, R_{red}, R_{blue} are atmospherically corrected or partially atmosphere-corrected (Rayleigh and ozone absorption) surface reflectance; L is the canopy background adjustment that addresses non-linear, differential NIR and red radiant transfer through a canopy; and C_1 and C_2 are the coefficients of the aerosol resistance term, which uses the blue band to correct for aerosol influences in the

red band. The coefficients adopted in the MODIS-EVI algorithm are: L = 1; C_1 = 6; C_2 = 7.5 and G (gain factor) = 2.5 (Huete et al. 2002).

2.1.1. *DisTrad-NDVI model for MODIS data*

Here, the DisTrad-NDVI model will be introduced by enhancing the spatial resolution of MODIS thermal images from 1000 m to 250 m. First, a NDVI image with 250-m resolution ($NDVI_{250}$) is made coarser to one with 1000-m resolution by nearest neighbour method. Using $NDVI_{250}$, the coefficient of variation (CV, the standard deviation divided by the mean) of each coarse pixel is computed. The $NDVI_{1000}$ pixels are divided into three groups: (1) 0<NDVI<0.2 (sparse canopy cover/bare land); (2) 0.2<NDVI<0.5 (partial canopy cover) and (3) NDVI>0.5 (high/full canopy cover). Then, a part of the pixels having the lowest CV is selected from each group because the relationship between NDVI-T_R in pure pixels at 1000-m resolution should be more closed to the relations at higher resolution image. In addition, a subset image should be extracted covering as many classes as possible to include higher dynamic ranges. Second, a least-squares fitting is performed relating T_R and $NDVI_{1000}$ values. Kustas et al. (2003) and Agam et al. (2007) pointed out that a linear equation between T_R and VI may be more suitable when T_R pixel size >1000-m resolution, as shown:

$$T'_{R1000}(NDVI_{1000}) = a + b \times NDVI_{1000} \tag{4}$$

where the 'superscript' symbol of T_R stands for an LST value linking the VIs regression equation. Here, the value was derived from MOD11A1 image in this article.

Third, in principle, Equation (4) could be used to estimate 250-m T_R, T'_R, directly by replacing $NDVI_{1000}$ with $NDVI_{250}$. However, the least-squares regression neglected the effects of variations in soil moisture (Agam et al. 2007). So, Equations (5) and (6) are suggested for correcting soil moisture:

$$\Delta T'_{R1000} = T_{R1000} - T'_{R1000} \tag{5}$$

$$T'_{R250}(i) = T'_{R1000}(NDVI_{250}(i)) + \Delta T'_{R1000} \tag{6}$$

where T_{R1000} is real LST with 1000-m resolution that was coarsened from ASTER product with 90-m resolution in this article, $\Delta T'_{R1000}$ is the difference between them, $T'_{R1000}(NDVI_{250}(i))$ is a LST value predicted using the parameter a and b in Equation (4), and $T'_{R250}(i)$ stands for the final estimate LST value with 250-m resolution.

2.1.2. *Modification of the DisTrad-NDVI model*

One modification to the DisTrad-NDVI model is replacing NDVI with F_c. After replacing NDVI with F_c, Agam et al. (2007) found that the precision of disaggregated pixels was higher than the results by the DisTrad-NDVI model, even at Landsat/ASTER pixel resolution. However, the actual precision of Agam's method is very low. One reason for this is that the study area of Agam et al. (2007) is different from that of Kustas et al. (2003). Consequently, it is difficult to conclude that the higher precision of Agam et al. (2007) is derived from the model modification or the land-cover changes of the study areas.

In this study, we also modified the DisTrad-NDVI model by replacing NDVI with EVI. Compared to NDVI and F_c, EVI has greater sensitivity in densely vegetated areas. In addition, EVI does not reach a saturated state easily. In addition, the step of canopy cover classification can be skipped in the DisTrad-NDVI model. To achieve replacing NDVI with EVI, we present the following calculated steps, and the meanings of parameters in Equations (7–10) are similar with Equations (4–6):

Step 1, a linear regression is performed relating EVI and T_R at 1000-m resolution:

$$T'_{R1000}(\mathrm{EVI}_{1000}) = a + b \times \mathrm{EVI}_{1000} \tag{7}$$

In Equation (7), values a and b can be calculated through regressions. Then, we can use EVI in each pixel (EVI_{1000}) to derive $T'_{R1000}(\mathrm{EVI}_{1000})$ and initially estimate values ($T'_{R1000}(\mathrm{EVI}_{250})$) in thermal pixels with 250-m resolution through Equation (8):

$$T'_{R1000}(\mathrm{EVI}_{250}) = a + b \times \mathrm{EVI}_{250} \tag{8}$$

Step 2, considering the effects of soil moisture variation, Equation (9) is used for correction:

$$\Delta T'_{R1000} = T_{R1000} - T'_{R1000} \tag{9}$$

Step 3, the surface temperature values of each pixel at 250-m resolution are calculated through Equation (10):

$$T'_{R250}(i) = T'_{R1000}(\mathrm{EVI}_{250}(i)) + \Delta T'_{R1000} \tag{10}$$

2.2. *Data*

The data in this article include synchronous data from two sensors of MODIS and ASTER in satellite Terra on 14 November 2007. The data from MODIS include two parts: the daily product MOD11A1 that contains LST with 1000 m (actually 926.625 m) resolution (LST1000) and the 16-day composite product MOD13Q1 that contains VIs with 250 m (actually 231.705 m) (NDVI250, EVI250). The ASTER data are ASTER level 2 surface temperature product AST_08 with 90-m resolution that have been atmospherically corrected (NASA 2001).

The study area is located in Ganzhou, Jiangxi Province, Southern China, which is a transition area of three mountains of Nanling, Wuyi and Zhuguang (Figure 1). This area belongs to the southern edge of a subtropical zone characterized by a wet monsoon climate. Adequate light and heat, a long growing reason, as well as abundant but unequal rainfall, makes it one of the commodity forest bases of Southern China. Forest tree species in the study area exhibit small differences in horizontal distribution, which makes it a typical densely vegetated area in Southern China.

The number of the area in VIs images with 250-m resolution is 86,832, in which the one with dense vegetation is 66,877, accounts for 77%. Compared to land-cover type product MCD12Q1 in 2007, on the basis of IGBP classification scheme, mixed forests is the main land cove type, and woody savannahs is the second biggest type in the area with NDVI >0.5 (Figure 2).

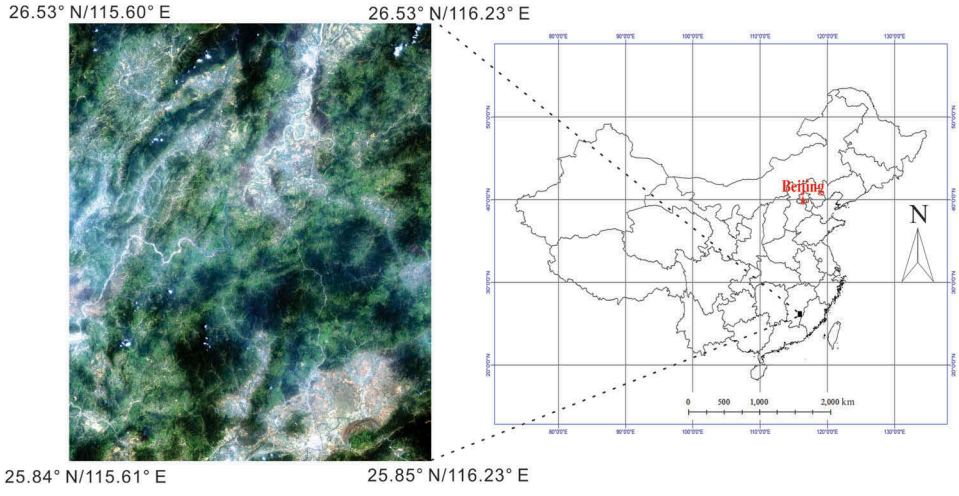

Figure 1. True colour image of the study area.

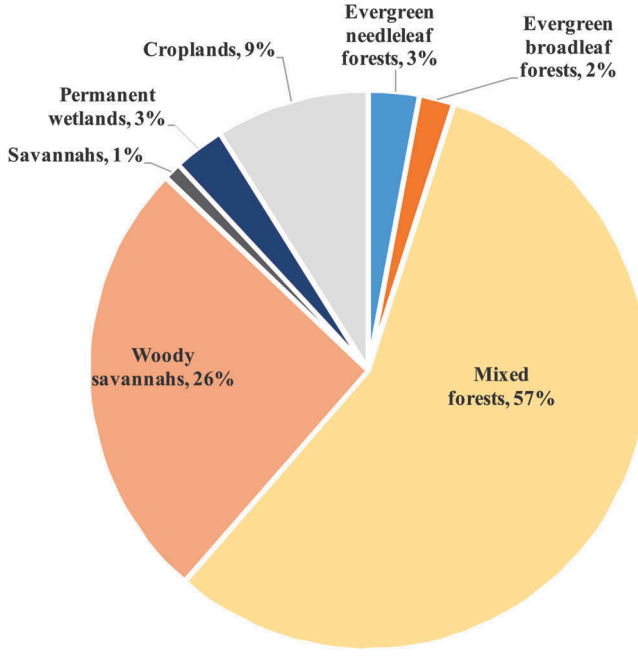

Figure 2. The land-cover type in densely vegetated areas of the study area.

In order to validate the results of the DisTrad-NDVI/EVI methods, ASTER high-resolution data (90 m) were used. ASTER data with 90-m resolution were transformed into radiation energy, registered with the final estimated image from MODIS (250 m). Then, a temperature image with the same resolution was calculated using the Planck formula. Finally, we can spatially coarsen an LST image from ASTER high-resolution data corresponding to the estimated LST image from MODIS data using the DisTrad-NDVI/EVI methods.

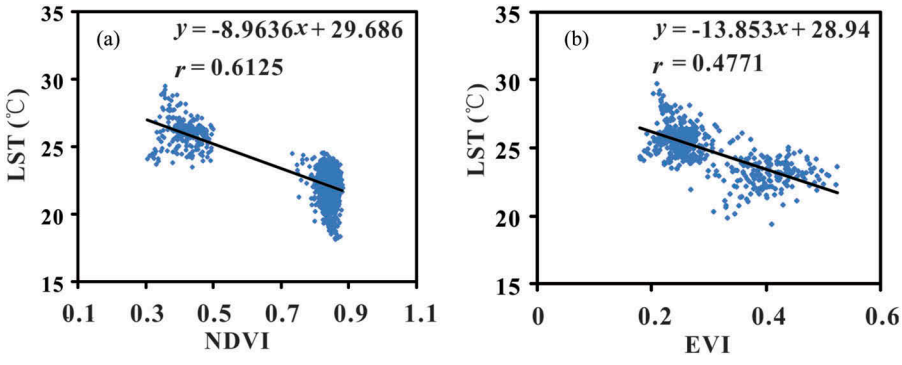

Figure 3. Linear fitting maps of VI-T_R: (a) Linear fitting between NDVI and T_R; (b) Linear fitting between EVI and T_R.

3. Results

3.1. *DisTrad-NDVI/EVI results*

Some suitable pixels that are classified by the above-mentioned steps are selected after $NDVI_{250}$ is resampled to $NDVI_{1000}$ with the same resolution as the LST image. A linear regression was performed between $NDVI_{1000}$ and LST, and the scatterplot was shown in Figure 3(a). Similarly, the same procedure was performed between EVI_{1000} calculated from EVI_{250} and LST, and the results were shown in Figure 3(b). Two linear equations, $T_R = -8.9636NDVI+29.686$ and $T_R = -13.853EVI+28.94$, were derived from linear regressions. $NDVI_{250}$, $NDVI_{1000}$, EVI_{250} and EVI_{1000} were used to calculate the surface temperature image, respectively.

We also calculated the difference ($\Delta T'_{R1000}$) between $T'_{R1000}(NDVI_{1000})$ and $T'_{R1000}(EVI_{1000})$, which is used for the correction of soil moisture. Finally, we calculated the LST image using the above results and Equations (4–10), which are shown in Figure 4, including the original thermal image in 1000-m resolution.

3.2. *Validation*

For validating the sub-pixel mapping results of thermal images of the DisTrad model, we compared the results with the synchronous 90-m thermal image from ASTER. First, we registered two images with some ground control points (GCPs) selected based on ground surface features. The GCPs must be selected carefully because the number and distribution of GCPs will influence the precision of registration. The overall error of the registration is approximately 0.623996, which is less than 1 pixel. The registered ASTER thermal image can be directly compared with the calculated thermal image using the DisTrad model.

3.3. *Statistical analysis*

For quantitatively evaluating the effects of sub-pixel mapping of thermal images of different methods, we conducted statistical analysis on one subset image. Figure 5 shows a comparison between an ASTER thermal image and MODIS thermal images calculated using the DisTrad-NDVI/EVI models. In general, three images are similar on

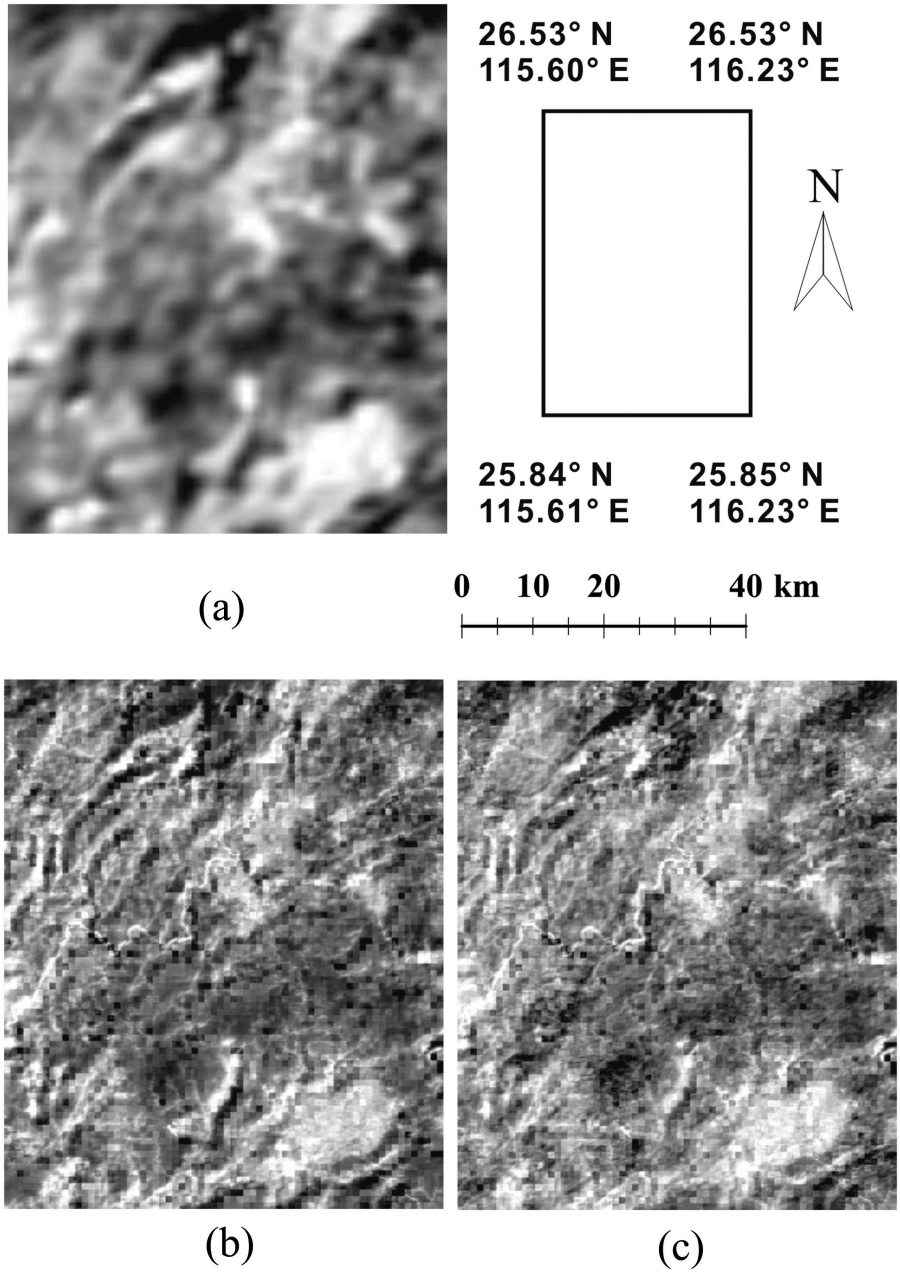

Figure 4. Comparison of the original and the calculated thermal image using the DisTrad-NDVI and DisTrad-EVI methods, respectively, in the study area: (a) Thermal image with 1000-m resolution; (b) thermal image in 250-m resolution derived from the DisTrad-NDVI method; (c) thermal image in 250-m resolution derived from the DisTrad-EVI method.

visual inspection. The thermal images calculated by the DisTrad-NDVI and DisTrad-EVI models appear very similar to the ASTER thermal image. Scatterplots in Figure 6 and three parameters in Table 2 show the DisTrad model is applicable for thermal sub-pixel mapping in Southern China. Compared to Table 2 from Kustas et al. (2003), the root

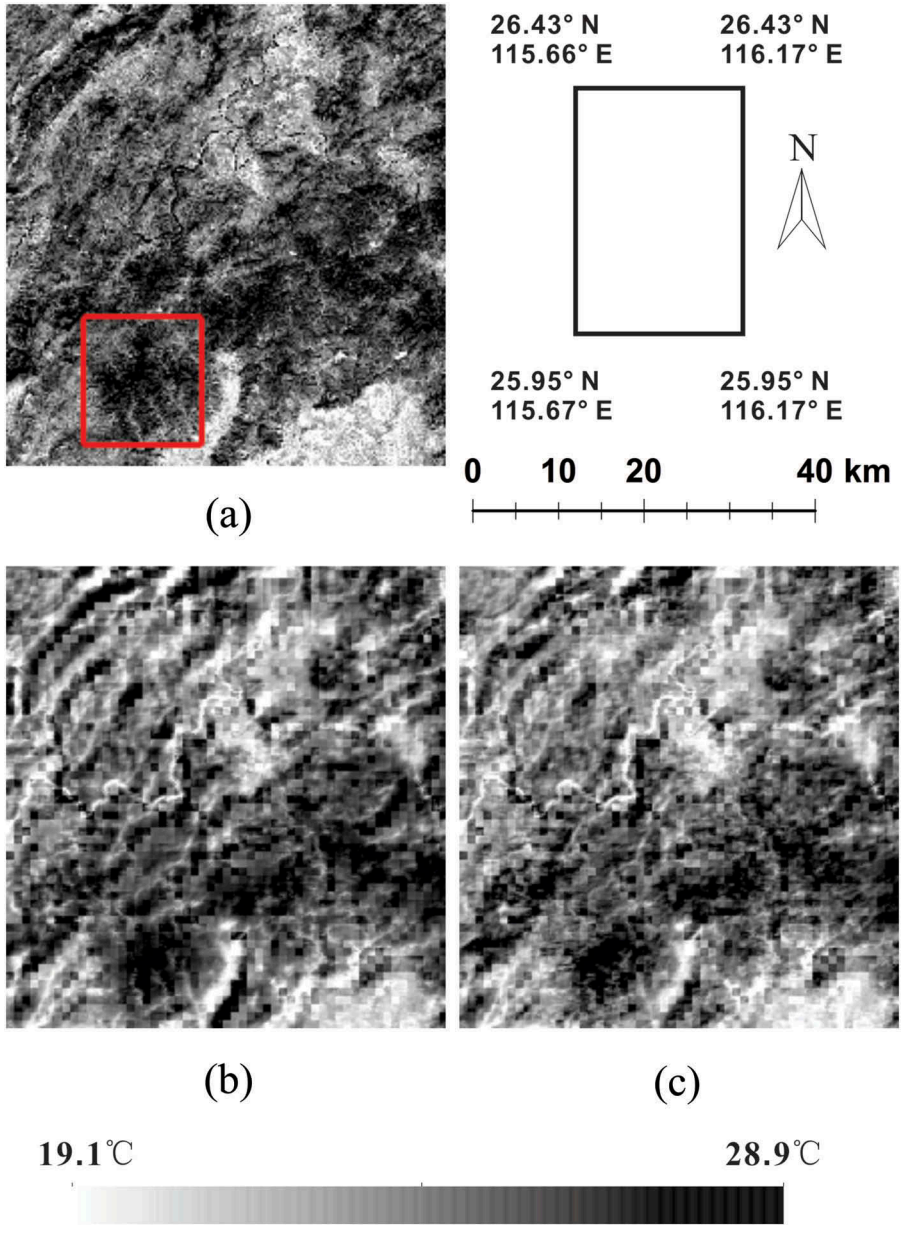

Figure 5. Comparison between ASTER and DisTrad-NDVI/EVI thermal images in subsets: (a) ASTER; (b) DisTrad-NDVI; (c) DisTrad-EVI.

mean square errors (RMSE) and correlation coefficients (*r*) are both acceptable (Table 2). And the mean difference of the DisTrad-EVI model is smaller than the one of DisTrad-NDVI model. It seems that the DisTrad-EVI model is more effective than DisTrad-NDVI. Here, a difference image between the registered ASTER thermal image and the two images by the DisTrad-NDVI and DisTrad-EVI models was calculated (Figure 7).

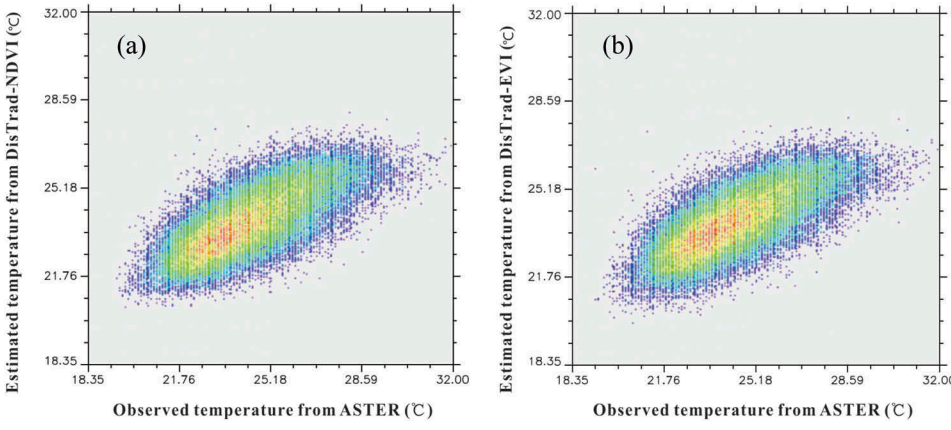

Figure 6. Scatterplots between ASTER image and DisTrad-NDVI and DisTrad-EVI images.

Table 2. Three parameters assessing the levels of the DisTrad-NDVI and DisTrad-EVI models using 89,216 points with respect to ASTER LST.

Model	RMSE	*r*	Mean difference
DisTrad-NDVI	1.581	0.676	0.047
DisTrad-EVI	1.549	0.680	0.043

The difference images are calculated using LST values from the ASTER image subtracted by the estimated LST values of the corresponding pixels, where yellow colour represents pixels with 4K lower LST values than the estimated values, while red colour represents pixels with 4K higher values than the estimated values. Generally, pixels with large differences are few, and proportions in two images of Figure 7 are less than 5% (4.23% in Figures 7(a) and 4.16% in Figure 7(b)). The distributions of pixels with large differences are similar in the two images, including both higher and lower ones. Here, the pixels with lower LST values are mostly in sub-area 1, while those with higher LST values are in located in sub-areas 2, 3 and 4. After a comparison with the high-resolution image, we found that the areas with large difference pixels were mostly non-vegetation areas in Figure 7. Specifically, sub-area 1 is water and sub-areas 2, 3 and 4 are build-up areas. This implies that the estimated LST values through NDVI or EVI are close to the actual temperature in vegetation areas, while the errors mostly appeared in non-vegetation areas.

In order to make a more clear comparison, a densely vegetated sub-area (shown by the red square in Figure 5(a)) was selected for analysis, and the results were shown in Figure 8 and Table 3. Compared to the ASTER thermal image, the DisTrad-EVI thermal image presents more precise and detailed information than the DisTrad-NDVI one. The boundaries between hills and bare lands are quite fuzzy in the DisTrad-NDVI image, and the internal area of vegetation (the dark blue zone in Figure 8(b)) is difficult to discern. Moreover, the temperature range of the DisTrad-NDVI image is from 21.1°C to 26.6°C with a difference of 5.5°C, which is much less than that of the ASTER thermal image (9.1°C). However, the temperature range of the DisTrad-EVI image varies from 19.6°C to 26.3°C with a difference of 6.7°C, which is broader than that of the DisTrad-NDVI image (Table 3). Inspecting the detailed distribution of LST in the ASTER image, the DisTrad-EVI image shows more detailed information of LST than the DisTrad-NDVI

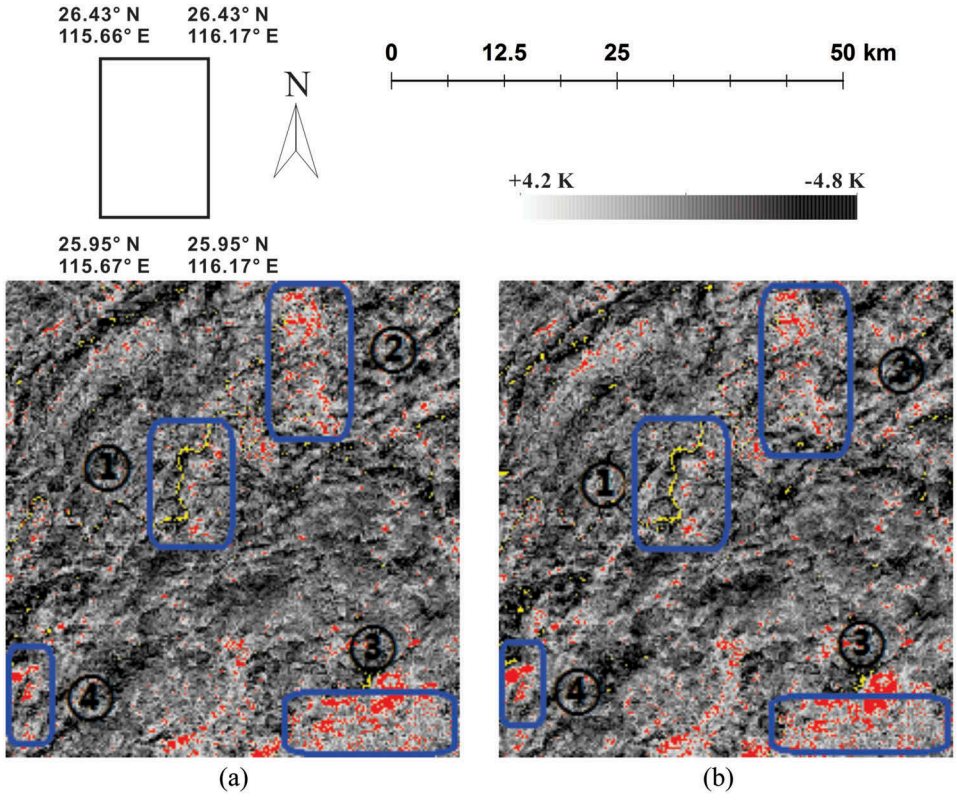

Figure 7. Comparison of images between the registered ASTER thermal image and two images by the DisTrad-NDVI and DisTrad-EVI methods, in which yellow colour represents pixels with 4K lower LST values than the estimated values, while red colour represents pixels with 4K higher values than the estimated values: (a) ASTER-(DisTrad-NDVI); (b) ASTER-(DisTrad-EVI).

image. This is consistent with the results of Huete et al. (2002), in which the NDVI tends to asymptotically saturate in densely vegetated regions, while the EVI remains sensitive to canopy variations.

Generally, the results of thermal sub-pixel mapping using either the DisTrad-NDVI or DisTrad-EVI model are not as good in non-vegetation areas. Regarding vegetation areas, both the DisTrad-NDVI and DisTrad-EVI model show good results for thermal sub-pixel mapping, which offers an important way for improving the spatial resolution of thermal remote-sensing images. Especially in densely vegetated areas, the DisTrad-EVI model is proven to be an effective way for thermal sub-pixel mapping, and promises wider applications than the DisTrad-NDVI one.

4. Conclusion and discussions

In this article, we compared the effect of NDVI and EVI in the DisTrad model for thermal sub-pixel mapping in densely vegetated areas due to their different sensitivity in densely vegetated areas. In an example area of Ganzhou, Southern China, a 250-m thermal

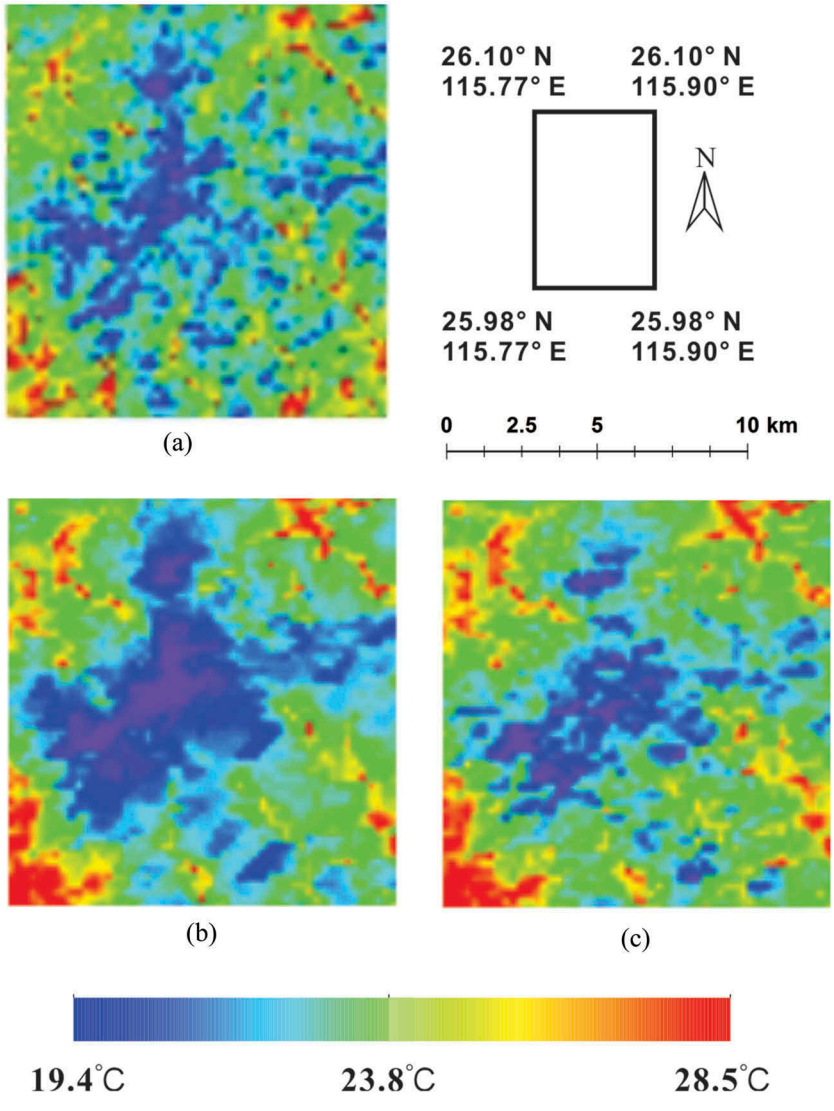

Figure 8. Comparison of thermal sub-pixel mapping of ASTER image (a), DisTrad-NDVI method (b) and DisTrad-EVI (c) in a high vegetation area.

Table 3. Temperature ranges of three temperature images in a high vegetation area.

Model	Lowest temperature (°C)	Highest temperature (°C)	Range (°C)
ASTER	19.4	28.5	9.1
DisTrad-NDVI	21.1	26.6	5.5
DisTrad-EVI	19.6	26.3	6.7

remote-sensing image from a 1000-m one was produced using 250-m EVI data. After comparing with the synchronous 90-m thermal image from ASTER, we drew the following conclusions:

(1) Because both NDVI and EVI are not sensitive to non-vegetation areas, the models of both DisTrad-NDVI and DisTrad-EVI are not good for thermal sub-pixel mapping in non-vegetation areas, such as water, bare soil and urban areas.
(2) Regarding middle-vegetation areas with sparse or partial canopies (e.g. NDVI<0.5), the DisTrad model using NDVI or EVI show very similar results.
(3) By substituting NDVI using EVI, the DisTrad model overcomes limitations in densely vegetated areas and exhibits wide applications in densely vegetated areas, such as Southern China, Southeast Asia and South America.
(4) Meanwhile, the step of canopy cover classification can be skipped in the DisTrad-EVI model. Therefore, the proposed DisTrad-EVI model is effective for thermal sub-pixel mapping in both dense- and rare-vegetation areas.

LST images with high temporal and high spatial resolutions are critical to regional and global research. This article proposed and validated the DisTrad-EVI model in densely vegetated areas. However, in non-vegetation areas, the DisTrad-EVI model is not recommended. Some indices that are sensitive to non-vegetation could be utilized to improve the DisTrad model applications in non-vegetation areas. In addition, the accumulation of errors will cause the uncertainty of temperature calculation when registered, which should also be considered in the DisTrad-EVI model.

Acknowledgements

Natural Science Foundation, NSFC (41401485), the China National Key Technology R&D Program (2012BAH32B03) and the China National 863 Program (2006AA06A306) are acknowledged for financial supports. Jake Carpenter of Beverly Hills English is thanked for the comments and corrections. This is contribution No. IS-2485 from GIGCAS.

Disclosure statement

No potential conflict of interest was reported by the authors.

Funding

This work was supported by NSFC [41401485]; the China National Key Technology R&D Program [2012BAH32B03]; China National 863 Program [2006AA06A306] and Natural Science Foundation.

References

Agam, N., W. P. Kustas, M. C. Anderson, F. Li, and C. M. U. Neale. 2007. "A Vegetation Index Based Technique for Spatial Sharpening of Thermal Imagery." *Remote Sensing of Environment* 107 (4): 545–558. doi:10.1016/j.rse.2006.10.006.

Choudhury, B. J., N. U. Ahmed, S. B. Idso, R. J. Reginato, S. Craig, and T. Daughtry. 1994. "Relations between Evaporation Coefficients and Vegetation Indices Studied by Model Simulations." *Remote Sensing of Environment* 50 (1): 1–17. doi:10.1016/0034-4257(94)90090-6.

Deng, W., Y. Q. Wan, and R. C. Zhao. 2001. "Detecting Coal Fires with a Neural Network to Reduce the Effect of Solar Radiation on Landsat Thematic Mapper Thermal Infrared Images." *International Journal of Remote Sensing* 22 (6): 933–944. doi:10.1080/014311601300074469.

Essa, W., B. Verbeiren, J. Van Der Kwast, T. Van De Voorde, and O. Batelaan. 2012. "Evaluation of the DisTrad Thermal Sharpening Methodology for Urban Areas." *International Journal of Applied Earth Observation & Geoinformation* 19 (1): 163–172. doi:10.1016/j.jag.2012.05.010.

Huete, A., K. Didan, T. Miura, E. P. Rodriguez, X. Gao, and L. G. Ferreira. 2002. "Overview of the Radiometric and Biophysical Performance of the MODIS Vegetation Indices." *Remote Sensing of Environment* 83 (1–2): 195–213. doi:10.1016/S0034-4257(02)00096-2.

Kogan, F. N. 2001. "Operational Space Technology for Global Vegetation Assessment." *Bulletin of the American Meteorological Society* 82 (9): 1949–1964. doi:10.1175/1520-0477(2001)082<1949:OSTFGV>2.3.CO;2.

Kustas, W. P., J. M. Norman, M. C. Anderson, and A. N. French. 2003. "Estimating Subpixel Surface Temperatures and Energy Fluxes from the Vegetation Index–Radiometric Temperature Relationship." *Remote Sensing of Environment* 85 (4): 429–440. doi:10.1016/S0034-4257(03)00036-1.

Lambin, E. F., and D. Ehrlich. 1996. "The Surface Temperature-Vegetation Index Space for Land Cover and Land-Cover Change Analysis." *International Journal of Remote Sensing* 17 (3): 463–487. doi:10.1080/01431169608949021.

Lv, Q. Q., J. H. Ding, and C. S. Cui. 2000. "Probable Satellite Thermal Infrared Anomaly before the Zhangbei M_S=6.2 Earthquake on January 10, 1998." *Acta Seismologica Sinica* 13 (2): 203–209. doi:10.1007/s11589-000-0011-1.

Merlin, O., B. Duchemin, O. Hagolle, F. Jacob, B. Coudert, G. Chehbouni, G. Dedieu, J. Garatuza, and Y. Kerr. 2010. "Disaggregation of MODIS Surface Temperature over an Agricultural Area Using a Time Series of Formosat-2 Images." *Remote Sensing of Environment* 114 (11): 2500–2512. doi:10.1016/j.rse.2010.05.025.

NASA. 2013. "Normalized Difference Vegetation Index (NDVI)." January 9. Accessed 9 January 2013. http://earthobservatory.nasa.gov/Features/MeasuringVegetation/measuring_vegetation_2.php

NASA, The Land Processes Distributed Active Archive Center (LP DAAC). 2001. "ASTER Level 2 Surface Temperature Product." Accessed 9 January 2013. https://lpdaac.usgs.gov. doi:10.5067/ASTER/AST_L1T.003.

Peng, G. X., L. I. Jing, Y. H. Chen, and A. P. Norizan. 2007. "A Forest Fire Risk Assessment Using ASTER Images in Peninsular Malaysia." *Journal of China University of Mining & Technology* 17 (2): 232–237. doi:10.1016/S1006-1266(07)60078-9.

Sandholt, I., K. Rasmussen, and J. Andersen. 2002. "A Simple Interpretation of the Surface Temperature/Vegetation Index Space for Assessment of Surface Moisture Status." *Remote Sensing of Environment* 79 (2–3): 213–224. doi:10.1016/S0034-4257(01)00274-7.

Sun, L., R. Sun, L. Xiaowen, S. Liang, and R. Zhang. 2012. "Monitoring Surface Soil Moisture Status Based on Remotely Sensed Surface Temperature and Vegetation Index Information." *Agricultural & Forest Meteorology* (166–167): 175–187. doi:10.1016/j.agrformet.2012.07.015.

Zakšek, K., and O. Krištof. 2012. "Downscaling Land Surface Temperature for Urban Heat Island Diurnal Cycle Analysis." *Remote Sensing of Environment* 117 (1): 114–124. doi:10.1016/j.rse.2011.05.027.

Zhan, W., Y. Chen, J. Zhou, J. Wang, W. Liu, J. Voogt, X. Zhu, J. Quan, and L. Jing. 2013. "Disaggregation of Remotely Sensed Land Surface Temperature: Literature Survey, Taxonomy, Issues, and Caveats." *Remote Sensing of Environment* 131 (8): 119–139. doi:10.1016/j.rse.2012.12.014.

Zhang, J., and Y. Wang. 2006. "A Pixel-Based Method to Estimate Urban Compactness and Its Preliminary Application." *International Journal of Remote Sensing* 27 (24): 5435–5442. doi:10.1080/01431160600983638.